



Graded-index breathing solitons from Airy pulses in multimode fibers

ZHIXIANG DENG,^{1,2} YU CHEN,¹ JUN LIU,^{1,3,*} CHUJUN ZHAO,⁴ AND DIANYUAN FAN¹

¹International Collaborative Laboratory of 2D Materials for Optoelectronics Science and Technology, Key Laboratory of Optoelectronic Devices and Systems of Ministry of Education and Guangdong Province, College of Optoelectronic Engineering, Shenzhen University, Shenzhen 518060, China

²School of Electrical Engineering, University of South China, Hengyang 421001, China

³Aston Institute of Photonic Technologies, School of Engineering and Applied Science, Aston University, Birmingham B4 7ET, UK

⁴Laboratory for Micro-/Nano- Optoelectronic Devices of Ministry of Education, IFSA Collaborative Innovation Center, School of Physics and Electronics, Hunan University, Changsha 410082, China

*j.liu26@aston.ac.uk

Abstract: Breathing solitons, as localized wave packets with a periodic evolution in amplitude and duration, are able to model extreme wave events in complex nonlinear dispersive systems. We have numerically studied the formation and manipulation of graded-index breathing solitons embedded in nonlinear multimode fibers based on a single nonlinear Schrödinger equation that includes the spatial self-imaging effect through a periodically varying nonlinear parameter. Through changing specific parameters of the input optical field, we can manipulate the period and depth of graded-index breathing soliton dynamics under different relative strengths between the dispersion length and the self-imaging period of the multimode fiber. Our study can explicitly derive a robust mechanism to control the behavior of the breathing localized structure directly and contribute to a better understanding of the much more complex nonlinear graded-index soliton dynamics in multimode fibers.

© 2019 Optical Society of America under the terms of the [OSA Open Access Publishing Agreement](#)

1. Introduction

Multimode waveguides, benefiting from an additional and new dimension in optical wave propagation, can arise with much richer qualitatively-new physical behaviors than that provided by a single spatial mode equivalent. They have attracted considerable attention in recent years regarding their applications in optical communication [1,2], spatial-temporal soliton dynamics [3], ultrafast photonics [4,5], and many other areas. Particularly, multimode fibers (MMFs) are becoming a promising solution to improve the capability of the next-generation telecommunication systems owing to the spatial division multiplexing technique [6]. Concerning the ultrafast photonics applications, the output power from multimode mode-locked fiber lasers where many longitudinal and transverse modes are coherently superimposed together to create ultrashort pulses [5], can be substantially scaled up compared to their traditional single-mode counterparts [7–9]. Different from the single-mode fibers, inside MMFs the nonlinear intermodal coupling effect is typically existing and can achieve a rich variety of spatiotemporal nonlinear effects [10–14] even though linear modal coupling like intermodal group dispersion is negligible. Whereas, the propagation dynamics of nonlinear optical pulses in a graded-index (GRIN) MMF, featuring very low inter-modal group dispersion and controllable spatiotemporal nonlinear effects, have aroused increasing interest in recent years [15–17]. In light of these previous investigations, a better and deeper understanding of the nonlinear soliton dynamics in MMFs is now imperative.

One of the most important subjects within nonlinear science is to investigate and explore the localized structures occurring in nonlinear physical systems. Breathing solitons, which are a fundamentally new form of self-localized structures featuring periodic oscillations in time

or space, can exist widely in nonlinear physical systems, such as Bose-Einstein condensates [18], granular lattices [19], hydrodynamics [20], optics [21] and so on. In contrast to traditional fundamental solitons with unchangeable temporal shape during the propagation, the breathing solitons experience compression and stretching regularly (periodically) in the time domain. Similar to Kuznetsov-Ma (KM) and Akhmediev breathers (ABs) predicted by the exact solutions of an underlying integrable model [21], breathing solitons are also related to the periodic energy exchange between the spectral components that are located at the center and the wings [22]. To date, the breathing soliton dynamics have been mainly investigated and explored in single-mode fibers [21] and optical microresonators [23–26]. It is worth noting that, the breathing state of solitons can also exist in MMFs since solitons composed of multiple spatial modes are able to experience a synchronized periodic oscillation in terms of amplitude and duration especially in GRIN MMFs with negligible intra-modal dispersion. More importantly, the investigation involving on the breathing soliton dynamics and corresponding mechanisms behind in MMFs will further extend their range of applications in different nonlinear physical systems and complete the fundamental theory of breathing soliton dynamics. However, the science and physics of optical breathing solitons in MMFs remain elusive, to the best of our knowledge, due to the three dimensional spatial features which add complexity to the simulation model [10,17]. Many questions about graded-index multimode breathers, such as the dynamics with spatial self-imaging effects included [8,12], are still raised to be solved. Recently, the stability of optical solitons in GRIN MMFs was studied in [27] to give a first fundamental understanding of the underlying multimode soliton dynamics by solving a single effective nonlinear Schrödinger equation (NLSE) derived by Conforti *et al* [28].

Besides, it is also worth noting that the wave packets in the form of Airy function have many unique properties in the nonlinear propagation media [29–31]. For example, the Airy pulses can be transformed into solitons and the excessive energy is shed into the low-intensity dispersive background radiation [29]. The interference process can be formed between them that gives rise to the observed oscillations [32]. Furthermore, the Airy pulses are able to move in a ballistic trajectory [33–35]. This means that the collision can occur between both temporally separated, co-propagating Airy pulses with in-phase. Hence, the stable bound and oscillating states can be achieved because of the momentum and energy exchange [36–38]. Therefore, the Airy pulses can be implemented to provide an appropriate technical route to observe the breathing soliton dynamics.

In this paper, we focus on forming and manipulating the typical localized wave packets of breathing soliton states in the nonlinear GRIN MMF system, aiming to present first insights into a fundamentally new type of multimode pulse dynamics. We find that the single soliton shedding from the Airy pulse can form the breathing state exhibiting a periodic oscillatory behavior. In addition, the breathing period and depth can be controlled by the peak power and truncation coefficient of the Airy pulse. We also discuss the generation dynamics of breathing solitons with a large frequency and depth created by the interaction between two shifted counter-propagating Airy pulses. Our results constitute a significant contribution to the emerging field of the complex spatiotemporal multimode systems that attracts growing interest in recent years.

2. Propagation model

With appropriate launching conditions in GRIN MMFs a large number of transverse modes can be excited, the spatial-temporal nonlinear propagation of which, as well as the overall superimposed field, can be modeled by the following Gross-Pitaevskii equation based on the paraxial and slowly varying envelope approximations [12,17,28]:

$$\frac{\partial E}{\partial z} = \frac{i}{2k_0} \left(\frac{\partial^2 E}{\partial x^2} + \frac{\partial^2 E}{\partial y^2} \right) - i \frac{\beta_2}{2} \frac{\partial^2 E}{\partial T^2} - i \frac{k_0 \Delta}{r^2} (x^2 + y^2) E + i \frac{n_2 \omega_0}{c} |E|^2 E \quad (1)$$

where E is the slowly varying electric-field envelope, $k_0 = n_0 \omega_0 / c$ is the wave number at ω_0 , r is the fiber core radius, Δ denotes the relative index difference between the cladding and the centre of the fiber, β_2 corresponds to the group-velocity dispersion, and n_2 is the Kerr coefficient. This equation can be numerically solved by the split-step Fourier-transform method [39], but requires a lot of computation time because of its (3 + 1) D nature.

In the linear or weakly/moderately nonlinear regime, the beam propagation in GRIN MMFs experiences the spatial self-imaging effect which is characterized by the periodic variation of specific beam parameters along the propagation distance [40,41]. In other words, when the injected field is a Gaussian beam the evolving optical field will remain approximately Gaussian while its width oscillates and recovers to its input value at certain distances. The amplitude of the known Gaussian beam takes the following form [27,28]:

$$|F(x, y, z)| = \frac{w_0}{w(z)} \exp \left[-\frac{1}{2} \frac{(x^2 + y^2)}{w^2(z)} \right] \quad (2)$$

$$w^2(z) = w_0^2 \left[\cos^2(\pi z / Z_p) + \frac{1-p}{(k_0^2 w_0^4) / Z_p} \sin^2(\pi z / Z_p) \right] \quad (3)$$

where w_0 is the spot size of the input beam, $p = n_2 \beta_0^2 w_0^2 P_0 / 2n_0$ is a dimensionless parameter associated with the beam collapse, and $Z_p = \pi r / \sqrt{2\Delta}$ is the spatial self-imaging period of a GRIN MMF at which the oscillated beam width w recovers to its initial value w_0 .

Assuming that during propagation the self-imaging pattern of the beam remains steady and the effect of nonlinearity on the self-imaging pattern can be neglected, the solution of Eq. (1) can be written as $E(x, y, z, T) = A(z, T) \cdot F(x, y, z)$. The (3 + 1) D problem can be reduced to the following quasi-one-dimensional NLSE that is much faster to solve:

$$\frac{\partial A}{\partial z} = -i \frac{\beta_2}{2} \frac{\partial^2 A}{\partial T^2} + i \gamma(z) |A|^2 A \quad (4)$$

where $A(z, T)$ is the pulse envelope, and the periodically varying nonlinear coefficient

$\gamma(z) = \frac{\omega_0 n_2}{2\pi c w^2(z)}$ indicates the spatial beam width oscillations of an input Gaussian beam

resulting from the GRIN-induced self-imaging effect. More details about the quasi-one-dimensional NLSE model developed by Conforti *at al.* can be found in their recent work [28].

It is common to normalize NLSE to describe the pulse propagation in fibers using the following dimensionless variables [39]:

$$\xi = z / L_D, \quad \tau = T / T_0, \quad U(\xi, \tau) = A(z, T) / \sqrt{P_0} \quad (5)$$

where ξ, τ and U correspond to the normalized propagation distance, time, and pulse envelope with regards to the dispersion length $L_D = T_0^2 / |\beta_2|$, initial pulse duration T_0 , and peak power P_0 , respectively. These give the following normalized NLSE:

$$\frac{\partial U}{\partial \xi} = -i \frac{1}{2} \frac{\partial^2 U}{\partial \tau^2} + i N^2 g(\xi) |U|^2 U \quad (6)$$

Here, $N = \sqrt{\gamma P_0 L_D}$ is the soliton order number, and the periodic function $g(\xi)$ is defined as

$$g(\xi) = 1 / [\cos^2(\pi q \xi) + C \sin^2(\pi q \xi)], \quad q = L_D / Z_p, \quad C = \frac{1-p}{(k_0^2 w_0^4) / Z_p} \quad (7)$$

It is worth noting that the optical pulse propagation dynamics have no qualitative difference for any values of C in the range 0.1-10 [27]. Here, we choose $C = 0.3$, showing that during each self-imaging cycle the beam width is compressed by a factor of nearly 1.8. The parameter q represents the ratio of the dispersion length to the spatial self-imaging period of a GRIN MMF. For a typical GRIN MMF ($r = 25 \mu\text{m}$, $\Delta = 0.01$, $n_2 = 3.2 \times 10^{-20} \text{m}^2/\text{W}$, $\beta_2 = -20 \text{ps}^2/\text{km}$ at the wavelength of around 1550 nm), the corresponding self-imaging period Z_p can be less than 1 mm while the fiber dispersion length L_D is more than 10 cm for $T_0 > 0.1$ ps. The resulting value of q is then greater than 100. Thus, within one dispersion length the spatial beam width will vary periodically with hundreds of times. Recently Ahsan *et al.* investigated the stability of optical solitons in GRIN MMFs as the spatial width can vary significantly compared to the temporal width [27]. The same approach can be used to predict the breathing evolution behavior of optical pulses inside GRIN MMFs. The selected two q values (100 and 1) in the simulation here correspond to the particular cases where the dispersion length is much larger than or just approaching the spatial self-imaging period. It should be noted that, the occasion of $q = 1$ does not actually exist where the temporal variation can remarkably affect the spatial oscillation of the beam. This q value can still be chosen and used for comparison to gain physical insight into complex spatial-temporal dynamics inside GRIN MMFs.

We need to stress that the most-complete model in GRIN MMFs is based on coupled modes theory of optical fields, which can decompose the solitons' spectrum into a sum of spatial functions associated with individual modes [17,42]. With the coupled-mode technique, one needs to handle the number of modes involved in calculations. Generally, large core MMFs can support several hundred of modes and thus the numerical calculations become time consuming and complex. The model adopted here allows the simulations of long fiber lengths with manageable computation time although the spatial evolution of the propagating beam cannot be studied. Recent studies show that this model is effective and numerically feasible when the injected optical field excites a large number of modes [13,28]. However, it cannot be used for studying multimode solitons composing of a few low-order modes.

3. Result and discussion

3.1 GRIN breathing solitons shedding from a single Airy pulse

Breathing solitons are a solitary wave in which energy is localized in time but oscillates in space, or vice versa. The quasi-one-dimensional NLSE with longitudinal varying nonlinear coefficient [43] provides an approach to simulate the spatiotemporal nonlinear dynamics, including the geometric parametric instability [12,16] or the ultra-broadband dispersive waves [3,13]. Particularly, it can also be used to predict the existence of stable GRIN breathing solitons in MMFs pumped by a finite-energy Airy pulse. The advantage of the Airy pulses with respect to conventional symmetric counterparts, such as Gaussian or Hyperbolic secant pulses, lies in that their spectral phase (the cubic term) introduces an additional degree of freedom for manipulation [29]. Here, we employ the exponentially decaying asymmetric Airy pulse as the injected light field, as follows:

$$U(\xi = 0, \tau) = \sqrt{R \cdot K(a)} \cdot Ai(\tau) \cdot \exp(a \cdot \tau) \quad (8)$$

where a ($0 < a < 1$) is the truncation coefficient, and $K(a)$ is a truncation-dependent normalized coefficient, and R is a dimensionless parameter that we can vary to scale the Airy pulse intensity.

Representative simulation results for the exponentially decaying Airy pulse ($R = 1$, $a = 0.3$) launched into a GRIN MMF are shown in Fig. 1. Figures 1(a) and 1(e) illustrate the dynamics of an Airy pulse in the temporal and spectral domains, respectively, under the situation where the dispersion length L_D is much larger than the spatial self-imaging period Z_p ($q = 100$). A soliton can be formed from the Airy pulse while its area obeys the soliton formation criterion [44]. It can be seen from Fig. 1(a) that the soliton cleans itself out by shedding a temporal continuum. The continuum traveling away from the soliton in both directions corresponds to the components that are moving faster or slower than the soliton. Similar to the fundamental solitons, these pulses can resist group-velocity dispersion and adjust adiabatically based on perturbations such as the periodically spatial oscillation induced by self-imaging. When the soliton is fully developed, the pulse starts to enter the breathing state showing periodical stretching and compression behaviors in the time domain. Figure 1(b) also shows that it takes about three dispersion lengths to accomplish the transition from an Airy pulse to the breathing soliton. Figure 2(a) shows the shortest and the longest temporal profiles when the soliton breathes. The temporal breathing ratio of the peak power is nearly 1.2. The broadest and narrowest spectra within the breathing state are shown in Fig. 2(b) for comparison, which also indicates that the intensity increases in the middle but decreases at both wings. It is a clear illustration of the energy exchange between the center and the wings.

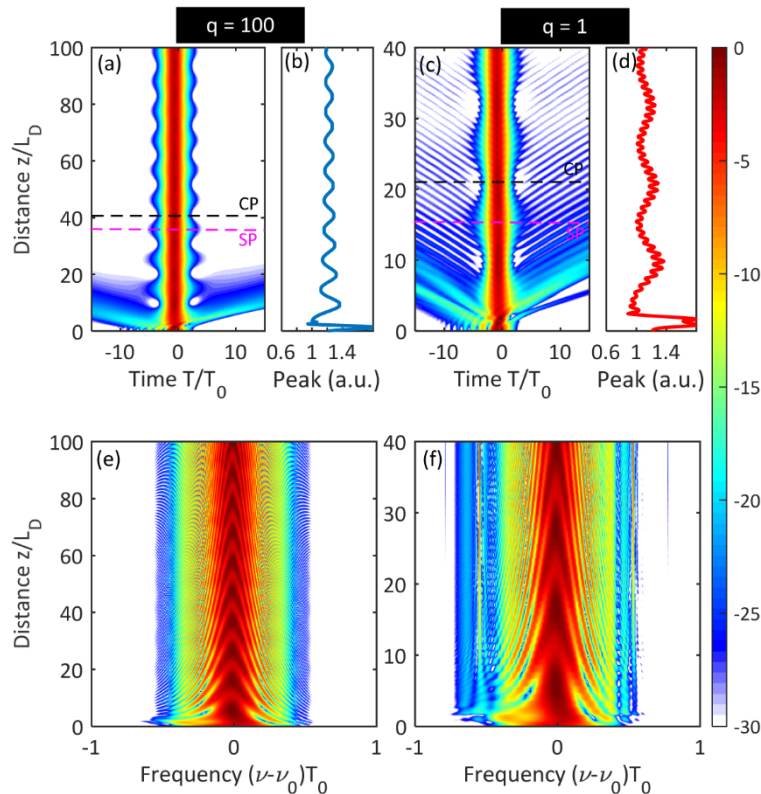


Fig. 1. Simulations of multimode breathing soliton dynamics. Temporal (top) and spectral (bottom) evolutions of the fundamental multimode soliton shedding from Airy pulses. Left column corresponds to the case of $q = 100$ while right column to $q = 1$. (b) and (d) show the peak power evolutions of the breathing solitons. In both cases, intensity is color-coded on a 30

dB scale. The periodic compression (CP) and stretching (SP) over one breathing period are indicated by a black dashed line and a red one, respectively.

For breathing solitons formed in a GRIN MMF, one significant difference from Akhmediev breathers (ABs) is that energy located in both wings of their spectrum can return to a set of spectral components around the central part [see Fig. 2(b)] in contrast to the corresponding energy returning to the single pump for ABs. This is attributed to the fact that the breathing soliton in the GRIN MMF is remaining as a single pulse during propagation, while the ABs totally recover to a continuous wave in Fermi-Pasta-Ulam recurrence [22]. This difference indicates how the breathing soliton dynamics in the framework of GRIN multimode waveguides are distinct from those in the single-mode waveguide and illustrates how the spatial self-imaging effects break the system's integrability and affect the breather behavior.

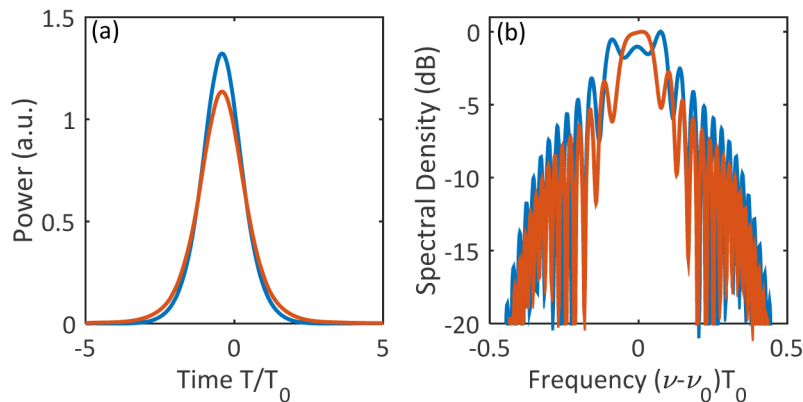


Fig. 2. Temporal and spectral profiles of the breathing soliton. The shortest and the longest temporal profiles (a) and the corresponding spectral profiles (b) for a multimode breathing soliton over one breathing cycle for the case shown in Fig. 1(a). The blue (brick-red) curve in the figure corresponds to the temporal and spectral profiles at the maximal compression (stretching) instant when the breathing soliton is excited.

The propagation dynamics of breathing solitons are also largely determined by the relative magnitude between the spatial self-imaging period Z_p and the dispersion length L_D . When Z_p approaches L_D (q approaches unity), resonant dispersive radiations can be emitted due to the soliton perturbation introduced by both of the characteristic spatial oscillation and the resulting periodic nonlinear coefficient [13,28]. The spectral component for these dispersive waves can be predicted by the resonance condition given in [45]. The temporal and spectral evolution of an injected Airy pulse with $q = 1$ are also elucidated given in Figs. 1(c) and 1(f), respectively. The periodic evolution over $40 L_D$ is still maintained acceptable despite that the breathing soliton is not stable in this limiting case. During the pulse evolution, the temporal profiles of the breathing solitons feature pulsating ripples but still remain sufficiently localized. It is not difficult to find from Fig. 1(c) that the dispersive waves that are periodically emitted away from the solitary wave are weakened gradually as the propagation distance increases. This is expected because the resonance can induce emission of dispersive waves until the amplitude of the solitary wave does not satisfy the resonance width determined by Z_p . From Fig. 1(d) we can see that the peak power evolution of the breathing soliton changes nearly periodically while the fast and irregular intensity oscillations can be identified for each breathing period. This behavior is similar to the pump power evolution for the parametric resonance breathers within the periodically modulated dispersion single-mode fiber [46]. These can be attributed to both the power decay in the form of the persistent dispersive wave emissions and the adiabatically reshaped pulse through the periodic perturbation given by $g(\xi)$ during each breathing cycle.

To gain deeper insight into the breathing dynamics of GRIN multimode solitons, we investigate and explore the relations between the amplitude modulations of formed breathing solitons and the intensity of the launched Airy pulse. The intensity of the launched Airy pulse can be given by:

$$E = \int_{-\infty}^{+\infty} |U(\xi = 0, \tau)|^2 d\tau = RK(a) \sqrt{\frac{1}{8\pi a}} \exp\left(\frac{2a^3}{3}\right), \quad (9)$$

which is highly dependent on two parameters, the pump laser power R and the truncation coefficient a . Figure 3(a) shows that the peak power of the breathing soliton as a function of the propagation distance for different pump power values R ranging from 0.9 to 1.2 when the truncation coefficient is fixed at 0.3. We define the breathing depth as $(P_{\max} - P_{\min}) / (P_{\max} + P_{\min})$, where $P_{\max(\min)}$ is the maximum (minimum) peak power during each breathing cycle. The soliton breathing depth and the breathing period are slightly decreasing with the launched power R . As is shown in Fig. 3(b), both the pulse breathing depth and period show a similar tendency as in Fig. 3(a) for the launched Airy pulse with a constant peak power R but the decreasing truncation coefficient a . This behavior is similar to the result in [29], where the dispersive waves in the form of excess energy shedding from the Airy pulse can have an impact on the evolved soliton breathing period through their interference effect. It is worth noting that with longer propagation distance this system can ultimately revert to a complex dynamical system that is approaching critical transitions. In the present case, the critical event exhibits the loss of single soliton induced by spatiotemporal instability.

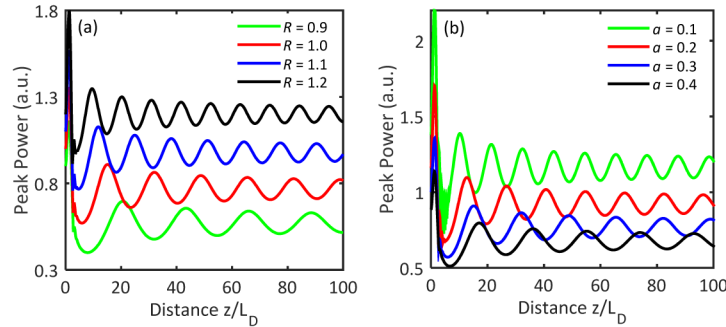


Fig. 3. Peak powers of the breathing soliton as a function of the propagation distance in terms of dispersion length for different launched peak powers R (a) and selected truncation coefficients a (b).

3.2 GRIN breathing solitons formed by the interaction of both Airy pulses with in-phase

Bright breathing solitons in GRIN MMFs are clearly observed and comprehensively modeled. The GRIN breathing soliton generally features a small breathing frequency (reciprocal of breathing period) and a weak breathing depth even after optimization through adjusting both the peak power and truncation coefficient of the incident Airy pulse. The Airy pulses are able to decelerate or accelerate (depending on their tail direction) during propagation based on their unique ballistic propagation feature [34] and allow for collisions between counter-propagating pulses with the same center frequency. To obtain breathing solitons with a high breathing frequency and depth, we consider the input optical fields that are consisted of a pair of well-separated counter-propagating Airy pulses with in-phase as follows:

$$U(\xi = 0, \tau) = \sqrt{R \cdot K(a)} \cdot \{Ai(\tau - T_1) \exp[a(\tau - T_1)] + Ai[-(\tau + T_1)] \exp[-a(\tau + T_1)]\}, \quad (10)$$

where arbitrary real constants T_1 stands for the time interval between both Airy pulses. For simplicity, we let $a = 0.2$ and $R = 1$ and only vary T_1 . Both Airy pulses can encounter and interact with each other in a ballistic route through adjusting T_1 , from which a soliton breathing state is then created with a high breathing frequency and depth.

Figure 4 shows the temporal and spectral evolution process of the interaction between in-phase Airy pulses with a temporal separation $T_1 = 2$ for different q values of 1 and 100. Although both counter-propagating Airy pulses are well separated by $2T_1$, the ballistic trajectories of Airy pulses would intersect and then strongly interact with each other through the nonlinearity modulated by the spatial oscillation. For $q = 100$, the two Airy components can form bound breathing solitons with a specific period. This is significantly different from multi-dimensional vector solitons formed by the interaction between in-phase solitons with separated frequencies in two degenerate LP11 modes of a step-index MMF [47]. As can be seen clearly from Figs. 4(a) and 4(c), the bound breathing state exhibits an oscillating structure with pulses breathing in both temporal and spectral domain as expected from higher-order soliton theory without perturbations [27]. In contrast, Figs. 4(b) and 4(d) present the simulation results in the case of $q = 1$. Owing to the bound soliton resonances [45] through the periodic perturbation induced by spatial self-imaging effect, the bound solitons in the compression stage are emitting dispersive radiations periodically until entering into the stretching stage. In the second compression stage, similar dispersive waves are emitted again while the bound solitons are splitting into two solitons with almost identical amplitude under resonant conditions.

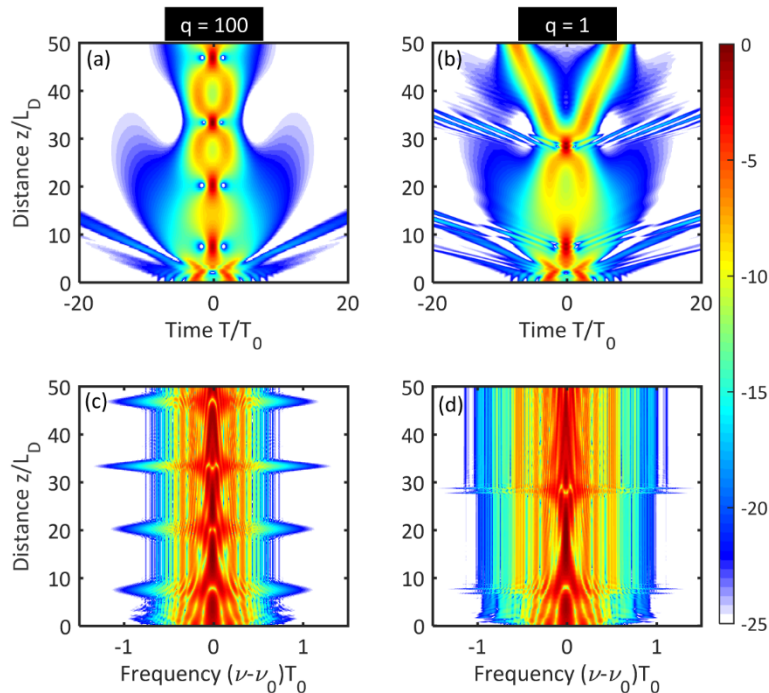


Fig. 4. Temporal (top) and spectral (bottom) evolutions over $50L_D$ for the interaction between both in-phase Airy pulses inside a GRIN MMF with $q = 100$ (a, c) and $q = 1$ (b, d). The intensity is coded on a decibel scale using dimensionless variables.

What we need to find out now is whether the bound breathing solitons propagate persistently and stably inside a GRIN MMF when a dispersion length L_D is much larger than the spatial self-imaging period Z_p . In this situation, we require to extend the propagation length of the bound solitons. In Figs. 5(a) and 5(b), we have observed such bound breathing

solitons propagating over one hundred dispersion lengths, which shows sufficient stability for the bound breathing solitons. Both temporal and spectral evolutions display the oscillation characteristics with a specific period. Different from the breathing dynamics of higher-order GRIN solitons [27], the periodic evolution pattern exhibited by the bound breathing solitons can be controlled by adjusting the initial time interval between both launched Airy pulses. The peak power versus the propagation distance is shown in Fig. 5(c) for varying initial time intervals T_1 . When the interval value ($|2T_1|$) is decreasing, the magnitude of the nonlinear interaction between two Airy components increases and the bound breathing solitons are formed with higher breathing frequency and depth. The highest breathing depth that can be obtained is about 40% [see the green curve in Fig. 5(c)]. It is worth noting that in the special case with $T_1 = 1$ the breathing frequency of formed bound states is the highest while its depth is smallest. We can attribute this to the following fact: the main lobes of both Airy pulses with $T_1 = 1$ are located at about zero and the generated solitons are directly shedding from the main lobes of Airy pulses, which is responsible for behaving along straight lines without the acceleration of the main lobes. This scenario corresponds to that of the second-order solitons, which are formed by two in-phase identical components superimposed in the temporal domain.

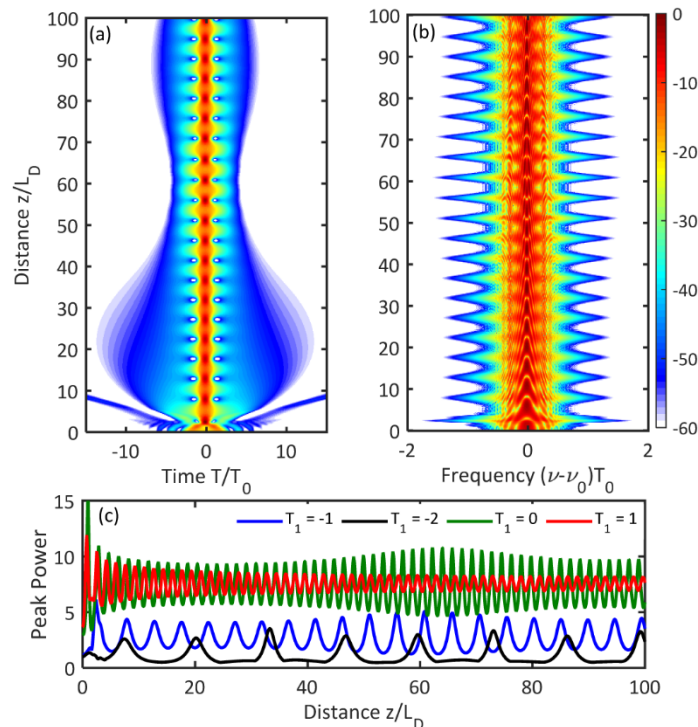


Fig. 5. Breathing solitons with a high breathing frequency and depth formed by the interaction between in-phase Airy pulses with varying time intervals in GRIN MMF. Temporal (a) and spectral (b) evolution of interaction between both Airy pulses with $T_1 = -1$. (c) Peak power of pulses versus propagation distance for different time intervals.

4. Conclusion

In conclusion, we have numerically demonstrated the formation and manipulation of breathing solitons in GRIN MMFs. Based on the variational method, the propagation dynamics of optical pulses within a GRIN MMF are modeled by a single NLSE including the spatial self-imaging effect through a longitudinally varying nonlinear coefficient. Results show that the breathing soliton can be excited from a single Airy pulse inside a GRIN fiber

under conditions where the dispersion length is much larger than or near the spatial self-imaging period. Depending on the peak power evolution of the input optical pulse and formed soliton, we find that the breathing soliton exhibits periodic stretching and compression in the temporal domain. Furthermore, the dispersive waves are periodically emitted away from the breathing solitons under the condition with $q = 1$. In view of the unique ballistic propagation feature of the Airy pulses, we consider the interaction between both time-reversal Airy pulses with in-phase to obtain the bound breathing states with a high breathing frequency and depth. By adjusting the time intervals between both launched Airy pulses the breathing frequency and depth of the corresponding bound states can be controlled. The obtained highest depth of breathing solitons is about 40%, which is close to the depth of breather solitons in an optical microresonator [24]. Our results can contribute to the understanding of the complex graded-index soliton dynamics and new spatiotemporal phenomena in nonlinear multimode fibers.

Funding

European Horizon 2020-MSCA-IF under Grant 701493, the National Natural Science Fund Foundation of China (NSFC) (Grants 61805115, 61875132, 61505124, 61505122, and 61606166), the Science and Technology Planning Project of Guangdong Province of China under Grant 2016KCXTD006, and Shenzhen Government's Plan of Science and Technology (Grant No. JCYJ20170302153731930).

References

1. H. R. Stuart, "Dispersive multiplexing in multimode optical fiber," *Science* **289**(5477), 281–283 (2000).
2. O. Tzang, A. M. Caravaca-Aguirre, K. Wagner, and R. Piestun, "Adaptive wavefront shaping for controlling nonlinear multimode interactions in optical fibres," *Nat. Photonics* **12**(6), 368–374 (2018).
3. L. G. Wright, D. N. Christodoulides, and F. W. Wise, "Controllable spatiotemporal nonlinear effects in multimode fibres," *Nat. Photonics* **9**(5), 306–310 (2015).
4. W. Fu, L. G. Wright, P. Sidorenko, S. Backus, and F. W. Wise, "Several new directions for ultrafast fiber lasers [Invited]," *Opt. Express* **26**(8), 9432–9463 (2018).
5. L. G. Wright, D. N. Christodoulides, and F. W. Wise, "Spatiotemporal mode-locking in multimode fiber lasers," *Science* **358**(6359), 94–97 (2017).
6. D. J. Richardson, J. M. Fini, and L. E. Nelson, "Space-division multiplexing in optical fibres," *Nat. Photonics* **7**(5), 354–362 (2013).
7. S. Fan and J. M. Kahn, "Principal modes in multimode waveguides," *Opt. Lett.* **30**(2), 135–137 (2005).
8. K. Krupa, A. Tonello, B. M. Shalaby, M. Fabert, A. Barthélémy, G. Millot, S. Wabnitz, and V. Couderc, "Spatial beam self-cleaning in multimode fibres," *Nat. Photonics* **11**(4), 237–241 (2017).
9. L. G. Wright, Z. Liu, D. A. Nolan, M. J. Li, D. N. Christodoulides, and F. W. Wise, "Self-organized instability in graded-index multimode fibres," *Nat. Photonics* **10**(12), 771–776 (2016).
10. L. G. Wright, W. H. Renninger, D. N. Christodoulides, and F. W. Wise, "Spatiotemporal dynamics of multimode optical solitons," *Opt. Express* **23**(3), 3492–3506 (2015).
11. J. Lægsgaard, "Spatial beam cleanup by pure Kerr processes in multimode fibers," *Opt. Lett.* **43**(11), 2700–2703 (2018).
12. K. Krupa, A. Tonello, A. Barthélémy, V. Couderc, B. M. Shalaby, A. Bendahmane, G. Millot, and S. Wabnitz, "Observation of geometric parametric instability induced by the periodic spatial self-imaging of multimode waves," *Phys. Rev. Lett.* **116**(18), 183901 (2016).
13. L. G. Wright, S. Wabnitz, D. N. Christodoulides, and F. W. Wise, "Ultrabroadband dispersive radiation by spatiotemporal oscillation of multimode waves," *Phys. Rev. Lett.* **115**(22), 223902 (2015).
14. K. Krupa, C. Louot, V. Couderc, M. Fabert, R. Guénard, B. M. Shalaby, A. Tonello, D. Pagnoux, P. Leproux, A. Bendahmane, R. Dupiol, G. Millot, and S. Wabnitz, "Spatiotemporal characterization of supercontinuum extending from the visible to the mid-infrared in a multimode graded-index optical fiber," *Opt. Lett.* **41**(24), 5785–5788 (2016).
15. R. Dupiol, A. Bendahmane, K. Krupa, J. Fatome, A. Tonello, M. Fabert, V. Couderc, S. Wabnitz, and G. Millot, "Intermodal modulational instability in graded-index multimode optical fibers," *Opt. Lett.* **42**(17), 3419–3422 (2017).
16. C. Mas Arabi, A. Kudlinski, A. Mussot, and M. Conforti, "Geometric parametric instability in periodically modulated graded-index multimode fibers," *Phys. Rev. A (Coll. Park)* **97**(2), 023803 (2018).
17. W. H. Renninger and F. W. Wise, "Optical solitons in graded-index multimode fibres," *Nat. Commun.* **4**(1), 1719 (2013).
18. A. Trombettoni and A. Smerzi, "Discrete solitons and breathers with dilute bose-einstein condensates," *Phys. Rev. Lett.* **86**(11), 2353–2356 (2001).
19. S. Flach and C. R. Willis, "Discrete breathers," *Phys. Rep.* **295**(5), 181–264 (1998).

20. A. Chabchoub, N. P. Hoffmann, and N. Akhmediev, "Rogue wave observation in a water wave tank," *Phys. Rev. Lett.* **106**(20), 204502 (2011).
21. J. M. Dudley, F. Dias, M. Erkintalo, and G. Genty, "Instabilities, breathers and rogue waves in optics," *Nat. Photonics* **8**(10), 755–764 (2014).
22. A. Mussot, C. Naveau, M. Conforti, A. Kudlinski, F. Copie, P. Szriftgiser, and S. Trillo, "Fibre multi-wave mixing combs reveal the broken symmetry of Fermi–Pasta–Ulam recurrence," *Nat. Photonics* **12**(5), 303–308 (2018).
23. M. Yu, J. K. Jang, Y. Okawachi, A. G. Griffith, K. Luke, S. A. Miller, X. Ji, M. Lipson, and A. L. Gaeta, "Breather soliton dynamics in microresonators," *Nat. Commun.* **8**, 14569 (2017).
24. E. Lucas, M. Karpov, H. Guo, M. L. Gorodetsky, and T. J. Kippenberg, "Breathing dissipative solitons in optical microresonators," *Nat. Commun.* **8**(1), 736 (2017).
25. C. Bao, L. Zhang, L. C. Kimerling, J. Michel, and C. Yang, "Soliton breathing induced by stimulated Raman scattering and self-steepening in octave-spanning Kerr frequency comb generation," *Opt. Express* **23**(14), 18665–18670 (2015).
26. H. Guo, E. Lucas, M. H. Pfeiffer, M. Karpov, M. Anderson, J. Liu, M. Geiselmann, J. D. Jost, and T. J. Kippenberg, "Intermode breather solitons in optical microresonators," *Phys. Rev. X* **7**(4), 041055 (2017).
27. A. S. Ahsan and G. P. Agrawal, "Graded-index solitons in multimode fibers," *Opt. Lett.* **43**(14), 3345–3348 (2018).
28. M. Conforti, C. Mas Arabi, A. Mussot, and A. Kudlinski, "Fast and accurate modeling of nonlinear pulse propagation in graded-index multimode fibers," *Opt. Lett.* **42**(19), 4004–4007 (2017).
29. Y. Fattal, A. Rudnick, and D. M. Marom, "Soliton shedding from Airy pulses in Kerr media," *Opt. Express* **19**(18), 17298–17307 (2011).
30. G. A. Siviloglou and D. N. Christodoulides, "Accelerating finite energy Airy beams," *Opt. Lett.* **32**(8), 979–981 (2007).
31. J. Broky, G. A. Siviloglou, A. Dogariu, and D. N. Christodoulides, "Self-healing properties of optical Airy beams," *Opt. Express* **16**(17), 12880–12891 (2008).
32. M. W. Chbat, M. N. Islam, C. E. Socolich, P. R. Prucnal, and J. P. Gordon, "Long-range interference effects of soliton reshaping in optical fibers," *J. Opt. Soc. Am. B* **10**(8), 1386–1395 (1993).
33. R. Driben, Y. Hu, Z. Chen, B. A. Malomed, and R. Morandotti, "Inversion and tight focusing of Airy pulses under the action of third-order dispersion," *Opt. Lett.* **38**(14), 2499–2501 (2013).
34. G. A. Siviloglou, J. Broky, A. Dogariu, and D. N. Christodoulides, "Ballistic dynamics of Airy beams," *Opt. Lett.* **33**(3), 207–209 (2008).
35. E. Greenfield, M. Segev, W. Walasik, and O. Raz, "Accelerating light beams along arbitrary convex trajectories," *Phys. Rev. Lett.* **106**(21), 213902 (2011).
36. X. Zhong, L. Chen, K. Cheng, N. Yao, and J. Sheng, "Generation of single or double parallel breathing soliton pairs, bound breathing solitons, moving breathing solitons, and diverse composite breathing solitons in optical fibers," *Opt. Express* **26**(12), 15683–15692 (2018).
37. M. Shen, J. Gao, and L. Ge, "Solitons shedding from Airy beams and bound states of breathing Airy solitons in nonlocal nonlinear media," *Sci. Rep.* **5**(1), 9814 (2015).
38. Y. Zhang, M. Belić, Z. Wu, H. Zheng, K. Lu, Y. Li, and Y. Zhang, "Soliton pair generation in the interactions of Airy and nonlinear accelerating beams," *Opt. Lett.* **38**(22), 4585–4588 (2013).
39. G. P. Agrawal, *Nonlinear Fiber Optics* (Academic, 2007).
40. S. Longhi and D. Janner, "Self-focusing and nonlinear periodic beams in parabolic index optical fibres," *J. Opt. B: Quantum Semiclass* **6**(5), S303–S308 (2004).
41. M. Karlsson, D. Anderson, and M. Desaix, "Dynamics of self-focusing and self-phase modulation in a parabolic index optical fiber," *Opt. Lett.* **17**(1), 22–24 (1992).
42. R. Khakimov, I. Shavrin, S. Novotny, M. Kaivola, and H. Ludvigsen, "Numerical solver for supercontinuum generation in multimode optical fibers," *Opt. Express* **21**(12), 14388–14398 (2013).
43. F. K. Abdullaev, S. A. Darmanyan, S. Bischoff, and M. P. Sørensen, "Modulational instability of electromagnetic waves in media with varying nonlinearity," *J. Opt. Soc. Am. B* **14**(1), 27–33 (1997).
44. H. A. Haus and W. S. Wong, "Solitons in optical communications," *Rev. Mod. Phys.* **68**(2), 423–444 (1996).
45. A. Hasegawa and Y. Kodama, "Guiding-center soliton," *Phys. Rev. Lett.* **66**(2), 161–164 (1991).
46. M. Conforti, A. Mussot, A. Kudlinski, S. Rota Nodari, G. Dujardin, S. De Bièvre, A. Armaroli, and S. Trillo, "Heteroclinic structure of parametric resonance in the nonlinear Schrödinger equation," *Phys. Rev. Lett.* **117**(1), 013901 (2016).
47. A. Mecozzi, C. Antonelli, and M. Shtaif, "Nonlinear propagation in multi-mode fibers in the strong coupling regime," *Opt. Express* **20**(11), 11673–11678 (2012).